Quantum signature for laser-driven correlated excitation of Rydberg atoms

Huaizhi Wu,[1,2] Yong Li,[3,4] Zhen-Biao Yang,[1,2] and Shi-Biao Zheng[1,2]

[1]*Department of Physics, Fuzhou University, Fuzhou 350116, People's Republic of China*

[2]*Fujian Key Laboratory of Quantum Information and Quantum Optics, Fuzhou University, Fuzhou 350116, People's Republic of China*

[3]*Beijing Computational Science Research Center, Beijing 100193, People's Republic of China*

[4]*Synergetic Innovation Center of Quantum Information and Quantum Physics, University of Science and Technology of China,*

Hefei, Anhui 230026, China

The excitation dynamics of a laser-driven Rydberg-atom system exhibits a cooperative effect due to the interatomic Rydberg-Rydberg interaction, but the large many-body system with inhomogeneous Rydberg coupling is hard to exactly solve or numerically study by density-matrix equations. In this paper, we find that the laser-driven Rydberg-atom system with most of the atoms being in the ground state can be described by a simplified interaction model resembling the optical Kerr effect if the distance-dependent Rydberg-Rydberg interaction is replaced by an infinite-range coupling. We can then quantitatively study the effect of the quantum fluctuations on the Rydberg excitation with the interatomic correlation involved and analytically calculate the statistical characteristics of the excitation dynamics in the steady state, revealing the quantum signature of the driven-dissipative Rydberg-atom system. The results obtained here will be of great interest for other spin-1/2 systems with spin-spin coupling.

I. INTRODUCTION

A laser-driven Rydberg gas in which the Rydberg excited atoms experience the long-range dipole-dipole or van der Waals interaction potential can exhibit atomic many-body correlations that are of great interest for future applications in quantum information processing [1] and quantum nonlinear optics [2]. While much attention has recently been devoted to the enhancement of optical nonlinearity by mapping the Rydberg-Rydberg correlation onto an optical field [3–13] and to the nonequilibrium quantum phenomena [14–20] and the preparation of Rydberg crystals [21–23] by modulating the driven-dissipative dynamics, quantitative understanding of the excitation process for the Rydberg-atom system itself is of particular interest, on the other hand, and is not yet clear.

There has been a lot of theoretical work focusing on the excitation dynamics in both the coherent [24–31] and dissipative regimes [32–40]. Generally, the system was analyzed via a mean-field treatment disregarding the interatomic correlation [18,19,23,32,38], a variational approach allowing for an approximation of the true steady state [39] or a perturbation theory up to fourth order [33,37,40]. Alternatively, the incoherent dynamics can be numerically simulated on account of strong dissipation via the rate equation [25,36] and weak decay via the density-matrix master equation [28] (or, equivalently, the wave-function Monte Carlo approach [33–36,38]) and the density-matrix renormalization group [22], which are normally useful for lattice geometries consisting of several tens of atoms.

The excitation dynamics under resonant and off-resonant driving exhibit different counting statistics of the Rydberg-atom number. While the resonant driving leads to a reduced number fluctuations of the Rydberg excitations [30,41,42], the off-resonant coupling offers richer physics such as the experimentally observed optical bistability [43], Rydberg aggregates [44,45], bimodal counting distribution [46], and kinetic constraints [47]. In addition, of special interest for

the experimental analysis is the formation mechanism of the collective many-body states since the statistical characteristics [44,46] and direct imaging [48,49] are challenging for distinguishing sequential and simultaneous excitation processes of Rydberg atoms. These have also been theoretically studied via the analytical model with generalized Dicke states [41] and Monte Carlo simulation [44].

In this paper, we study the excitation dynamics of a laser-driven dissipative Rydberg-atom system in the Holstein-Primakoff regime; that is, the majority of the atoms remain in the ground state [44,46]. To give an intuitive understanding, we make use of a simplified picture for the many-body system as in Ref. [34], where the characteristic C_μ/R^μ ($\mu = 3,6$) dependent interaction for atom pairs with the separation R is replaced by an infinite-range coupling (or average pair interaction). It allows us to regard the system as a nonlinear optical polarizability model [50] and quantitatively study the effect of quantum correlations on the excitation dynamics in the steady state. We find from the linearized calculation that the quantum fluctuations to the first order will enhance the Rydberg population [34,37] and modulate the fluctuation of the collective excitation number. Moreover, the nonclassical effects like pair excitation of Rydberg atoms can be clearly revealed by the full quantum results after comparison with the classical steady-state solution. The limitations for this simplified model are also discussed. Our finding not only connects to the recent experimental observations for the many-body system with Rydberg-Rydberg coupling [51] but also relates to the trapped spin-1/2 ions system where the spin-spin couplings are mediated by the motional degrees of freedom [52].

This paper is organized as follows. In Sec. II, we introduce our model for the interacting Rydberg atoms in the Holstein-Primakoff regime. In Sec. III, we numerically solve the classical Langevin equation of motion for the Rydberg-atom system to study the bistability of Rydberg population. In

Sec. IV, we discuss the effect of quantum fluctuations on the Rydberg excitation dynamics in the linearized regime. In Sec. V, we give the exact steady-state solution of the Fokker-Planck equation for describing the full quantum dynamics. Section VI finally contains a summary of our results and an open discussion of the limitations for the model.

II. THEORETICAL MODEL

Consider a system of N atoms ($N \gg 1$) that are excited from the ground state $|g_j\rangle$ to a Rydberg state $|e_j\rangle$ by a continuous and spatially uniform laser beam with detuning Δ from atomic resonance and Rabi frequency Ω (assumed to be real). By including the all-to-all interatomic coupling (or average pair interaction) χ, the Hamiltonian in the interaction picture and rotating-wave approximation reads ($\hbar = 1$) [34]

$$H = \sum_{j=1}^{N} \left[-\Delta |e_j\rangle\langle e_j| + \frac{\Omega}{2}(|e_j\rangle\langle g_j| + |g_j\rangle\langle e_j|) \right]$$
$$+ \chi \sum_{j<k} |e_j\rangle\langle e_j| \otimes |e_k\rangle\langle e_k|. \quad (1)$$

We now introduce the collective spin operators $S^+ = \sum_{j=1}^{N} |e_j\rangle\langle g_j|$ and $S^- = \sum_{j=1}^{N} |g_j\rangle\langle e_j|$, which, according to the Holstein-Primakoff transformation, can be expressed in terms of the bosonic operators b and $b^\dagger$ (with $[b,b^\dagger] = 1$) as $S^+ = b^\dagger \sqrt{N - b^\dagger b}$ and $S^- = \sqrt{N - b^\dagger b} b$ if the lowest energy level of these new operators is set to be the atomic state in which all of the atoms are in the ground state [53,54]. It follows that $\sum_{j=1}^{N} |e_j\rangle\langle e_j| = \frac{1}{2}[S^+, S^-] + \frac{N}{2} = b^\dagger b$ and $\sum_{j<k} |e_j\rangle\langle e_j| \otimes |e_k\rangle\langle e_k| = \frac{1}{2} b^\dagger b^\dagger bb$. We then focus on the parameter regime where the mean number of Rydberg excitations is much less than the total number of atoms (i.e., $\bar{n}_e \equiv \langle b^\dagger b \rangle \ll N$), resulting in $S^+ \simeq \sqrt{N} b^\dagger$, $S^- \simeq \sqrt{N} b$ [44,46]. Thus, the Hamiltonian of the system can be rewritten by

$$H_b = -\Delta b^\dagger b + \frac{\chi}{2} b^\dagger b^\dagger bb + \lambda(b + b^\dagger), \quad (2)$$

with $\lambda = \sqrt{N}\Omega/2$. Note that the system involving the Rydberg-Rydberg coupling behaves in a way resembling the optical Kerr nonlinearity, and its coherent dynamics will remain in the symmetric Dicke-state space. However, the spontaneous decay from the Rydberg excited state (with the relaxation rate γ) may lead to an incoherent mixture with the asymmetric dark states. For clarity, our work will focus on the state space spanned mainly by null and single Rydberg excitations accompanied by a tiny fraction of double excitations. The Rydberg population is confirmed by direct simulations of the master equation $\dot{\rho} = -i[H_b, \rho] + \frac{\gamma}{2}(2b\rho b^\dagger - \rho b^\dagger b - b^\dagger b \rho)$ for a zero-temperature thermal reservoir, and the counting statistics of Rydberg excitation is quantified by the Mandel Q parameter defined as $Q = \langle(\Delta \hat{n}_e)^2\rangle/\langle\hat{n}_e\rangle - 1$, with $\hat{n}_e \equiv b^\dagger b$, as shown in Fig. 1. The exact simulation of the dissipative dynamics for few atoms with the Hamiltonian (1) can be found in Appendix A, which shows good agreement with the bosonization model. But it should also be mentioned that for a realistic Rydberg system, such as an atomic ensemble or a spin lattice, the finite interaction range and the continuum
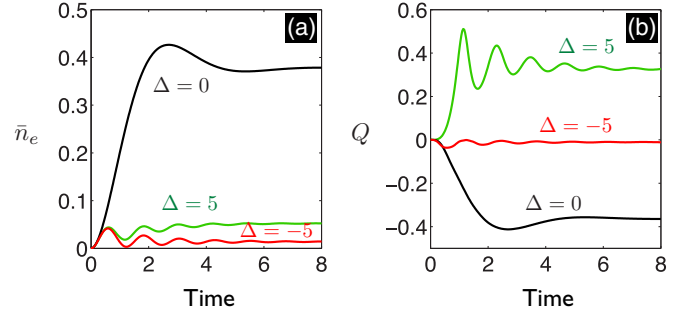

FIG. 1. (a) Mean Rydberg population $\bar{n}_e$ and (b) Mandel Q parameter as a function of time for laser detunings $\Delta = -5$, 0, and 5. We fix units of $\gamma = 1$, taking $\lambda = 0.6$, $\chi = 10$. In all cases the population of the double-excitation state is less than 0.01. For $\Delta = 5$, the Rydberg excitation exhibits super-Poissonian counting statistics with $Q > 0$, while for $\Delta = -5$ and $\Delta = 0$, the sub-Poissonian processes characterized by $Q < 0$ are found.

of interatomic coupling strengths due to broad distribution of atom positions may induce loss of interatomic correlations, which may negate the effectiveness of the model.

III. CLASSICAL DYNAMICS

The quantum Langevin equation of motion for the bosonic system is

$$\dot{b} = -i\lambda - i\Gamma b - i\chi b^\dagger b^2 + \xi(t), \quad (3)$$

where $\Gamma = -(\Delta + i\gamma/2)$ might include the decoherence due to the laser linewidths and Doppler broadening and $\xi(t)$ is the zero-value-mean noise operator. Beyond the mean-field theory, here the correlation between atoms is retained in the evolutional dynamics. In the classical limit, the equations of motion for $\bar{\alpha} = \langle b \rangle$ and $\bar{\alpha}^* = \langle b^\dagger \rangle$ are given by

$$\dot{\bar{\alpha}} = -i\lambda - i\bar{\alpha}(\Gamma + \chi|\bar{\alpha}|^2),$$
$$\dot{\bar{\alpha}}^* = i\lambda + i\bar{\alpha}^*(\Gamma^* + \chi|\bar{\alpha}|^2). \quad (4)$$

Then, the mean number of Rydberg excitations $\bar{n}_{es} = |\bar{\alpha}_s|^2$ in the steady state fulfills the algebraic equation

$$\chi^2 \bar{n}_{es}^3 - 2\chi\Delta\bar{n}_{es}^2 + \bar{n}_{es}|\Gamma|^2 - \lambda^2 = 0, \quad (5)$$

which allows at most three real positive roots. A stable $\bar{n}_{es}$ must conform to the Hurwitz criterion [given by $\partial(\lambda^2)/\partial\bar{n}_{es} = 3\chi^2\bar{n}_{es}^2 - 4\bar{n}_{es}\chi\Delta + |\Gamma|^2 > 0$ here], which ensures that the system returns to the stable branch soon after the small perturbation. Therefore, if the conditions $|\Delta| > \sqrt{3}\gamma/2$ and $\Delta\chi > 0$ are satisfied, the bistable region will be given by $\bar{n}_{es} > \bar{n}_{es}^{(+)}$ or $\bar{n}_{es} < \bar{n}_{es}^{(-)}$ with the real positive $\bar{n}_{es}^{(\pm)} = (2\Delta \pm \sqrt{\Delta^2 - \frac{3}{4}\gamma^2})/3\chi$. For our interest, the dependence of $\bar{n}_{es}$ on the laser detuning Δ for a repulsive interatomic interaction ($\chi > 0$) is shown in Fig. 2(b), which exhibits optical bistability with hysteresis [43]. The coexistence of low and high Rydberg populations in the off-resonance regime ($\Delta > 0$) leads to the bimodal counting distributions of the Rydberg excitation [46]. However, for $\Delta = 0$, the bimodality cannot arise due to the impossible bistability.
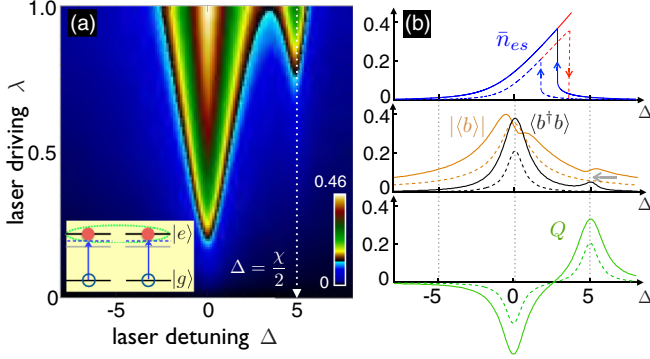
FIG. 2. (a) Mean number of Rydberg excitations $\langle b^\dagger b \rangle$ in the steady state with full quantum theory as a function of λ and Δ. The inset shows the pair excitation of two atoms for $\Delta = \chi/2$. (b) Classical stationary mean $\bar{n}_{es}$, quantum- mechanical steady-state solution of $\langle b^\dagger b \rangle$ and $|\langle b \rangle|$, and Mandel Q parameter versus laser detuning Δ with $\lambda = 0.3$ (dashed lines) and $\lambda = 0.6$ (solid lines). Other parameters are as in Fig. 1. χ, λ, and Δ are in units of γ.

IV. LINEARIZED DYNAMICS

The dissipative quantum dynamics for the system can be described by the master equation or the corresponding Fokker-Planck equation (FPE) [50],

$$\dot{P}(\alpha,\beta,t) = i\left[\frac{\partial}{\partial\alpha}(\Gamma\alpha + \chi\alpha^2\beta + \lambda) - \frac{\chi}{2}\frac{\partial^2}{\partial\alpha^2}\alpha^2 \right.$$
$$\left. - \frac{\partial}{\partial\beta}(\Gamma^*\beta + \chi\beta^2\alpha + \lambda) + \frac{\chi}{2}\frac{\partial^2}{\partial\beta^2}\beta^2 \right]P(\alpha,\beta,t),$$
$$(6)$$

by introducing the nondiagonal generalized P representation defined by

$$\rho(t) = \int_D d\sigma(\alpha,\beta)P(\alpha,\beta,t)\frac{|\alpha\rangle\langle\beta^*|}{\langle\beta^*|\alpha\rangle},\qquad (7)$$

where D is the integration domain and $d\sigma$ is the integration measure, which can be a volume integral $d^2\alpha d^2\beta$ over a complex phase space or a line integral $d\alpha d\beta$ over a manifold embedded in a complex phase space [50]. Note that α and β are arguments of the generalized P function (in relation to the c numbers of b and $b^\dagger$) and are complex conjugate in the mean $\bar{\alpha} = \bar{\beta}^*$.

Transforming the FPE into the Ito form yields a pair of stochastic differential equations (SDEs):

$$\frac{\partial}{\partial t}\begin{bmatrix} \alpha \\ \beta \end{bmatrix} = \begin{bmatrix} -i(\Gamma\alpha + \chi\alpha^2\beta + \lambda) \\ i(\Gamma^*\beta + \chi\beta^2\alpha + \lambda) \end{bmatrix}$$
$$+ \begin{bmatrix} -i\chi\alpha^2 & 0 \\ 0 & i\chi\beta^2 \end{bmatrix}^{\frac{1}{2}} \begin{bmatrix} \xi_1(t) \\ \xi_2(t) \end{bmatrix}, \qquad (8)$$

with $\xi_{1,2}(t)$ being the δ-correlated Gaussian white noise, satisfying $\langle \xi_{1,2}(t) \rangle = 0$ and $\langle \xi_{1,2}(t)\xi_{1,2}(t') \rangle \sim \delta(t - t')$. We then linearize the SDEs around the classically steady-state solution $\bar{\alpha}_s (\bar{\beta}_s = \bar{\alpha}_s^*)$ and find that the quantum fluctuation $\delta\hat{\mathbf{X}} = [\delta\hat{\alpha}, \delta\hat{\beta}]^T$ close to the classical stable branches obeys

the equation

$$\delta\dot{\hat{X}} = -\boldsymbol{\mu}(\bar{\alpha}_s) \cdot \delta\hat{\mathbf{X}} + \mathbf{D}^{1/2}(\bar{\alpha}_s) \cdot \boldsymbol{\xi}(t), \qquad (9)$$

where

$$\boldsymbol{\mu}(\bar{\alpha}_s) = -i\begin{bmatrix} \Gamma + 2\chi|\bar{\alpha}_s|^2 & -\chi\bar{\alpha}_s^{*2} \\ \chi\bar{\alpha}_s^2 & -\Gamma - 2\chi|\bar{\alpha}_s|^2 \end{bmatrix} \qquad (10)$$

and

$$\mathbf{D}(\bar{\alpha}_s) = \begin{bmatrix} -i\chi\bar{\alpha}_s^2 & 0 \\ 0 & i\chi\bar{\alpha}_s^{*2} \end{bmatrix} \qquad (11)$$

are the linearized drift and the diffusion array, respectively. The correlation matrix with regard to $\delta\hat{\mathbf{X}}$ can now be calculated through

$$\mathbf{C} = \begin{bmatrix} \langle b^2 \rangle - \langle b \rangle^2 & \langle b^\dagger b \rangle - |\langle b \rangle|^2 \\ \langle b^\dagger b \rangle - |\langle b \rangle|^2 & \langle b^{\dagger 2} \rangle - \langle b^\dagger \rangle^2 \end{bmatrix}$$
$$= \frac{\mathbf{D} \cdot \text{Det}(\boldsymbol{\mu}) + [\boldsymbol{\mu} - \mathbf{I} \cdot \text{Tr}(\boldsymbol{\mu})]\mathbf{D}[\boldsymbol{\mu} - \mathbf{I} \cdot \text{Tr}(\boldsymbol{\mu})]^T}{2\text{Tr}(\boldsymbol{\mu})\text{Det}(\boldsymbol{\mu})}. \qquad (12)$$

The above result allows us to obtain the mean Rydberg population and the Mandel Q parameter in the linearized regime (see Appendix B):

$$\bar{n}_e \approx |\bar{\alpha}_s|^2 + \langle \delta\hat{\alpha}^\dagger \delta\hat{\alpha} \rangle = \bar{n}_{es} + \frac{\chi^2}{2\Lambda}\bar{n}_{es}^2, \qquad (13)$$

$$Q \approx 2\bar{n}_{es}\text{Re}[\langle \delta\hat{\alpha}^2 \rangle / \bar{\alpha}_s^2] + 2\langle \delta\hat{\alpha}^\dagger \delta\hat{\alpha} \rangle$$
$$= \frac{\bar{n}_{es}\chi}{\Lambda}(\Delta - \chi\bar{n}_{es}), \qquad (14)$$

with $\Lambda = |\Gamma|^2 - 4\chi\Delta\bar{n}_{es} + 3\chi^2\bar{n}_{es}^2$. The steady-state solution $\bar{n}_{es}$ can be obtained by solving the set of classically nonlinear equations (4), and there may exist two stable solutions for a well-selected laser detuning, as shown in Fig. 2(b). We now assume this solution has been found and focus on the effect of the quantum fluctuations. One of the intriguing effects can be found in the asymptotic expansion of $\bar{n}_e$ to the first order [see Eq. (13)], where the Rydberg population is enhanced by the Rydberg-Rydberg coupling via the intensity of the quantum fluctuation $\langle \delta\hat{\alpha}^\dagger \delta\hat{\alpha} \rangle$ [34,37]. Second, due to the Rydberg-Rydberg interactions, the laser field drives the atomic transition from the ground state to the Rydberg state in a cooperative manner, with the fluctuations of the collective excitation number being characterized by the Mandel Q factor. The results show that the collective excitation number exhibits super-Poissonian distribution for laser detuning Δ greater than the collective energy shift $\bar{n}_{es}\chi$ among the correlated interacting particles ($\Delta/\bar{n}_{es}\chi > 1$) and sub-Poissonian distribution for the other case, (i.e., $\Delta/\bar{n}_{es}\chi < 1$), leading to collective quantum jumps while the system stays in the two classically stable branches [34]. The linear theory breaks down for $\Lambda \to 0$ (corresponding to the violation of the Hurwitz criterion), in which case $\bar{n}_{es}$ approaches the onset of instability.

V. FULL QUANTUM DYNAMICS

Having seen the effect of the quantum fluctuations based on the linearization, we next address the question with full quantum theory. In the quantum noise limit, there exists an

exact steady-state solution $P_{ss}(\alpha,\beta) = \alpha^{c-2}\beta^{d-2} \exp[-z(1/\alpha + 1/\beta) + 2\alpha\beta]$ for the FPE (6), with $z = 2\lambda/\chi$, $c = 2\Gamma/\chi$, and $d = c^*$ (see Appendix C). While we obtain the generalized P function, the Rydberg population and the Rydberg counting statistics can be calculated via

$$\langle b^{\dagger n}b^m \rangle = \frac{\int_D d\sigma(\alpha,\beta)P_{ss}(\alpha,\beta)\beta^n\alpha^m}{\int_D d\sigma(\alpha,\beta)P_{ss}(\alpha,\beta)}. \tag{15}$$

The appropriate integration domain D here will be a complex manifold embedded in the space $\mathbb{C}^2$, and each path of integration is chosen to be a Hankel path $\mathcal{O}$. These ensure that the distribution function $P(\alpha,\beta)$ vanishes correctly at the boundary. Skipping over the fussy calculations, we finally come to (see Appendix C)

$$\langle b \rangle = \frac{z}{c} \frac{{}_0F_2(c+1,d,2z^2)}{{}_0F_2(c,d,2z^2)}, \tag{16}$$

$$\langle b^{\dagger}b \rangle = \frac{z^2}{cd} \frac{{}_0F_2(c+1,d+1,2z^2)}{{}_0F_2(c,d,2z^2)}, \tag{17}$$

$$Q = \frac{z^2}{(c+1)(d+1)} \frac{{}_0F_2(c+2,d+2,2z^2)}{{}_0F_2(c+1,d+1,2z^2)}$$
$$- \frac{z^2}{cd} \frac{{}_0F_2(c+1,d+1,2z^2)}{{}_0F_2(c,d,2z^2)}, \tag{18}$$

where ${}_0F_2(c,d,z)$ is a hypergeometric series defined as

$$ {}_0F_2(c,d,z) = \sum_{n=0}^{\infty} \frac{z^n}{n!} \frac{\Gamma(c)\Gamma(d)}{\Gamma(c+n)\Gamma(d+n)}, \tag{19}$$

with $\Gamma(x) = [\frac{z^{1-x}}{2\pi i} \int_{\mathcal{O}} \sigma^{-x}e^{\sigma z}d\sigma]^{-1}$ being the gamma function.

The phase diagram for the mean number of Rydberg excitations in (λ,Δ) space shows that the Rydberg excitation dramatically increases at the laser detunings $\Delta = 0$ and $\Delta = \chi/2$ [see Fig. 2(a)], which corresponds to individually resonant excitation of each atom and pair excitation of the interacting atoms, respectively. Numerical simulation proves that the system is confined in the subspace spanned by the null- and double-excitation states for $\Delta = \chi/2$ without considering the relaxation, confirming that for this detuning the atomic excitation is caused by the two-photon process; this is fundamentally different from the case of resonant driving, where the system has no probability of being pumped to the state with more than one excitation due to the Rydberg blockade. Taking into account the atomic spontaneous emission, the issue of whether the many-body states of the Rydberg atoms are created by the coherent two-photon process or sequential excitations of individual atoms is then determined by the sequential excitation to the two-photon ratio, which is proportional to $\gamma^2/N\Omega^2$ [44]. Thus, the system favors double excitation since the multiatom coherence becomes significant and the dephasing induced by random distribution of atom positions and the specific spatial laser profile is neglected [36]. This can be further confirmed by measuring the Mandel Q parameter that is in close relation to the spatial correlation function $g^{(2)}(R)$ [55]. The excitation processes exhibit sub-Poissonian character ($Q < 0$) on resonance and super-Poissonian character ($Q > 0$) for $\Delta = \chi/2$. In addition, due to the fact that the interatomic correlations between any pair of atoms are included, the cooperative transitions from the double-excitation state to the
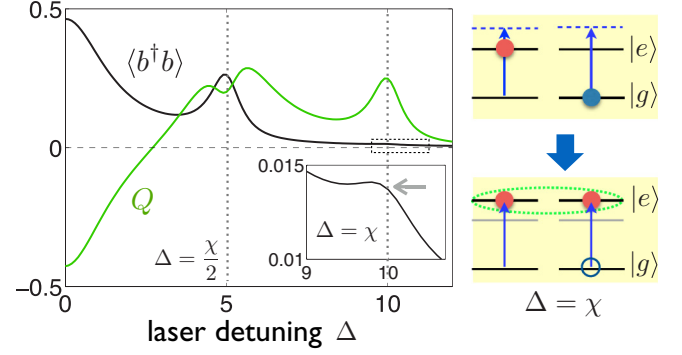

FIG. 3. Left: Quantum-mechanical steady-state solution of mean Rydberg population $\langle b^{\dagger}b \rangle$ and Mandel Q parameter versus laser detuning Δ with increasing driving strength $\lambda = 1$ and $\chi = 10$. χ, λ, and Δ are in units of γ. Right: An already excited Rydberg atom forwards the excitation of the surrounding atoms interacting with it for $\Delta = \chi$. See the text for details.

higher-excitation states are largely detuned from resonance and are suppressed because the collective energy shifts are much larger than the laser driving strength.

For $0 < \Delta < \chi/2$, both the individual excitation and the pair excitation are possible. While the classical dynamics predicts an optical bistability, the quantum-mechanical calculation including the interatomic correlation does not exhibit bistability. It should also be noted that the pair excitation of two atoms is a nonclassical effect that cannot be revealed by the classical theory [see arrow in Fig. 2(b); see also Appendix D]. An extra quantum signature for the system is given by the dips in the laser-detuning dependence of $|\langle b \rangle|$, which arise at the transition points of the Mandel Q factor, which shows reduced or enhanced quantum fluctuations of Rydberg excitations [16,32,34].

Increasing the laser intensity will enhance the mean number of Rydberg excitations for $\Delta = \chi/2$ but meanwhile weaken the super-Poissonian excitation process due to the decreasing ratio $\Delta/\bar{n}_{es}\chi$, as shown in Fig. 3. This fact can be directly understood from the linearized calculation [Eq. (14)]. For the far-off-resonance regime $\Delta \gg \Omega$, there is a small chance (roughly $N\Omega^2/4\Delta^2$) for an atom to be excited to the Rydberg state if all the atoms are initially in the ground state. However, while an atom has been luckily excited by the laser beam with the detuning $\Delta = \chi$, similar to the Rydberg aggregates, the surrounding atoms tend to be excited cooperatively due to the Rydberg-Rydberg coupling, as sketched in the right panel of Fig. 3. Also, the sequential to simultaneous three-photon excitation ratio is on the order of $\gamma^2\Delta^2/N^2\Omega^4$ and is extremely weak here.

VI. DISCUSSION AND CONCLUSION

As mentioned in Sec. II, the simplified picture here requires the interatomic correlations to be well preserved in the whole Rydberg ensemble, and the only scenario where the present model describes actual Rydberg-atom interactions is when all interactions are so strong ($\chi \gg \Delta$ or λ) that the ensemble is fully blockaded; that is, not even double excitations can ever occur. While the scale of a Rydberg-atom system is much larger than the blockade radius (i.e., the critical correlation

distance), the quantum correlations may vanish for Rydberg atoms located far away from each other; then the situation becomes different for the Rydberg excitation number related to the number of blockade spheres that fit into the excitation volume. The excitation dynamics for an ultracold Rydberg gas with high atomic density has been experimentally studied in the strong-dephasing regime (due to the spatial dependence of atom positions or laser geometry) and in the limit of short excitation times [44,46].

It is more interesting to study the excitation dynamics in the scenario where χ is of an order comparable to Δ or λ, as employed here. The quantum correlations among all the atoms become essential, giving rise to the pronounced quantum signature discussed previously. But for actual experiments such as individual Rydberg atoms trapped in tunable two-dimensional arrays of optical microtraps [51], the distance-dependent interatomic coupling strength is determined by the specific lattice sites that the atoms locate on, and therefore the factor of 8 (or higher) difference in interactions comparing two adjacent atoms already introduces correlations and breaks the present approach. This is regardless of the dimensionality or geometry of the lattice. However, the strong two-photon transitions will still be visible while many pairs of atoms feature a distance that fits in with the two-photon resonance condition; namely, the two-photon resonance can be enhanced by choosing the appropriate detuning for a given lattice constant [36]. The limitations arise from the fact that the atoms near the edge of the lattice evolve as an inhomogeneous distribution of atom positions, which breaks the spatial symmetry and may induce an additional dephasing, reducing the visibility of two-photon transitions [51].

In conclusion, we have analyzed the steady-state excitation dynamics of a weakly driven Rydberg-atom system by treating the inhomogeneous Rydberg-Rydberg interaction as an all-to-all coupling. While the present model cannot represent the full picture of a realistic system, in contrast to the previous analytical or experimental studies that mainly focus on the mean-field dynamics and neglect the interatomic correlations, the analytical calculation here allows us to find the effect of the quantum fluctuations on the Rydberg excitation process and the quantum phenomena such as simultaneous biexcitation of Rydberg atoms and interaction-assisted Rydberg excitation, which are referred to as the quantum signature of the system. The simplified model forms the basis for quantitatively understanding the Rydberg aggregates [44,45], bimodal counting distribution [46], and kinetic constraints [47] in recent experimental observations with Rydberg atoms and, more generally, the many-body effect for the interacting spin-1/2 systems [52].
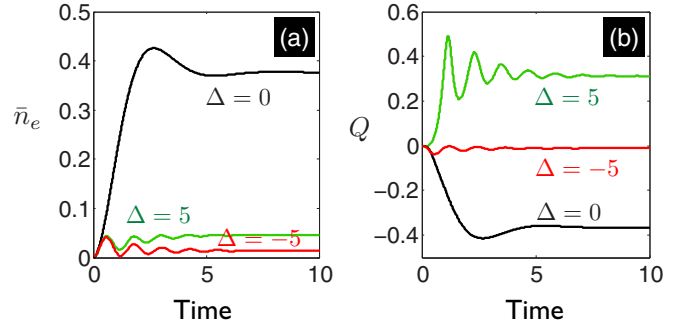
FIG. 4. (a) Mean Rydberg population $\bar{n}_e$ and (b) Mandel Q parameter as a function of time for laser detunings $\Delta = -5$, 0, and 5. Other parameters are as in Fig. 1.

APPENDIX A: THE EXACT SIMULATION OF THE DISSIPATIVE DYNAMICS WITH ATOMIC SPIN OPERATORS

In this appendix, we show that the exact simulation of the Hamiltonian H in the main text with spin operators for few atoms is found to be in good agreement with the theoretical model in terms of bosonic operators. We also show how to obtain the correlation matrix under linearization and the analytical steady-state solution for the Fokker-Planck equation as in Ref. [50], discussing the optical bistability for the nonlinear polarizability model. The nonclassical nature of the quantum-mechanical steady states is also shown by the Wigner functions.

The exactly dissipative dynamics of the laser-driven system with the Hamiltonian H in the main text can be described by the master equation

$$\dot{\rho} = \frac{1}{i\hbar}[H,\rho] + \frac{\gamma}{2}\sum_{j=1}^{N}\mathcal{L}_j, \qquad (A1)$$

where

$$\mathcal{L}_j = 2\sigma_{ge}^{(j)}\rho\sigma_{eg}^{(j)} - \sigma_{eg}^{(j)}\sigma_{ge}^{(j)}\rho - \rho\sigma_{eg}^{(j)}\sigma_{ge}^{(j)}, \qquad (A2)$$

$\sigma_{ge}^{(j)} = |g_j\rangle\langle e_j|$, and $\sigma_{eg}^{(j)} = |e_j\rangle\langle g_j|$. With the excitation-number operator being $\hat{n}_e = \sum_{j=1}^{N}|e_j\rangle\langle e_j|$, the mean number of Rydberg excitations and the Mandel Q parameter can be calculated via $\bar{n}_e = \text{Tr}(\rho\hat{n}_e)$ and $Q = \text{Tr}[\rho(\Delta\hat{n}_e)^2]/\text{Tr}(\rho\hat{n}_e)-1$, respectively.

Simulating Eq. (A1) with $N = 6$, we show the time-dependent mean Rydberg population $\bar{n}_e$ and Mandel Q parameter in Fig. 4 and the steady-state solution of $\bar{n}_e$ and Q versus laser detuning Δ in Fig. 5, which demonstrate the quantitatively good agreement with the results obtained via the simulation of the bosonization model.

APPENDIX B: THE QUANTUM FLUCTUATION UNDER LINEARIZATION

Splitting the operators b ($b^\dagger$) into classical and quantum parts $\alpha = \bar{\alpha} + \delta\hat{\alpha}(t)$, $\beta = \bar{\beta} + \delta\hat{\beta}(t)$ ($\bar{\alpha}^* = \bar{\beta}$), we obtain the
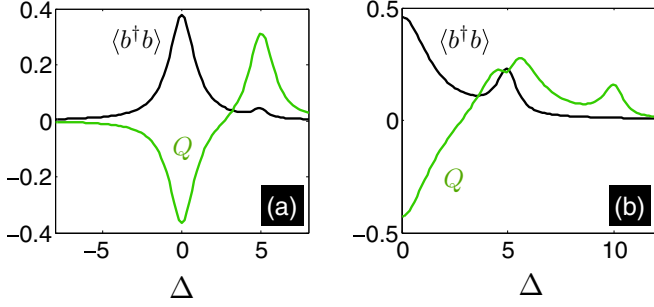
FIG. 5. Quantum-mechanical steady-state solution of $\bar{n}_e$ and Mandel Q parameter versus laser detuning Δ for (a) $\lambda = 0.6$ and (b) $\lambda = 1$. Other parameters are as in Fig. 2(b).

linearized correlation matrix given by

$$
\mathbf{C} = \begin{bmatrix} \langle b^2 \rangle - \langle b \rangle^2 & \langle b^\dagger b \rangle - |\langle b \rangle|^2 \\ \langle b^\dagger b \rangle - |\langle b \rangle|^2 & \langle b^{\dagger 2} \rangle - \langle b^\dagger \rangle^2 \end{bmatrix}
$$

$$
= \begin{bmatrix} \langle \delta \hat{\alpha}^2 \rangle & \langle \delta \hat{\alpha}^\dagger \delta \hat{\alpha} \rangle \\ \langle \delta \hat{\alpha}^\dagger \delta \hat{\alpha} \rangle & \langle \delta \hat{\alpha}^{\dagger 2} \rangle \end{bmatrix}, \tag{B1}
$$

where

$$
\langle \delta \hat{\alpha}^2 \rangle = -\frac{\chi \bar{\alpha}^2 (\Gamma^* + 2\chi \bar{n}_{es})}{2\Lambda}, \tag{B2}
$$

$$
\langle \delta \hat{\alpha}^\dagger \delta \hat{\alpha} \rangle = \frac{\chi^2 \bar{n}_{es}^2}{2\Lambda}, \tag{B3}
$$

and

$$
\langle \delta \hat{\alpha}^{\dagger 2} \rangle = -\frac{\chi \bar{\alpha}^{*2} (\Gamma + 2\chi \bar{n}_{es})}{2\Lambda}, \tag{B4}
$$

with $\Lambda = \frac{\gamma^2}{4} + \Delta^2 - 4\chi \Delta \bar{n}_{es} + 3\chi^2 \bar{n}_{es}^2$, obtained from $\mathbf{C} = \frac{\mathbf{D} \cdot \mathrm{Det}(\boldsymbol{\mu}) + [\boldsymbol{\mu} - \mathbf{I} \cdot \mathrm{Tr}(\boldsymbol{\mu})] \mathbf{D} [\boldsymbol{\mu} - \mathbf{I} \cdot \mathrm{Tr}(\boldsymbol{\mu})]^T}{2 \mathrm{Tr}(\boldsymbol{\mu}) \mathrm{Det}(\boldsymbol{\mu})}$ by using the drift and diffusion arrays. Thus, the mean number of Rydberg excitations and the Mandel Q parameter in the linearized regime are given by

$$
\bar{n}_e \approx |\bar{\alpha}|^2 + \langle \delta \hat{\alpha}^\dagger \delta \hat{\alpha} \rangle = \bar{n}_{es} + \frac{\chi^2}{2\Lambda} \bar{n}_{es}^2 \tag{B5}
$$

and

$$
Q = \frac{[\langle (b^\dagger b)^2 \rangle - \langle b^\dagger b \rangle^2]}{\langle b^\dagger b \rangle} - 1
$$

$$
= \frac{2\mathrm{Re}[\bar{\alpha}^{*2} \langle \delta \hat{\alpha}^2 \rangle] + 2\bar{n}_{es} \langle \delta \hat{\alpha}^\dagger \delta \hat{\alpha} \rangle}{\bar{n}_{es} + \langle \delta \hat{\alpha}^\dagger \delta \hat{\alpha} \rangle} + O[(\delta \hat{\alpha}^\dagger)^2 (\delta \hat{\alpha})^2], \tag{B6}
$$

respectively. For $\langle \delta \hat{\alpha}^\dagger \delta \hat{\alpha} \rangle \ll \bar{n}_{es}$ and keeping only the first-order fluctuation, the Mandel Q parameter approximates to

$$
Q \approx 2\mathrm{Re}[\langle \delta \hat{\alpha}^2 \rangle / \bar{\alpha}^2] + 2\langle \delta \hat{\alpha}^\dagger \delta \hat{\alpha} \rangle
$$

$$
= \frac{\bar{n}_{es} \chi}{\Lambda} (\Delta - \chi \bar{n}_{es}). \tag{B7}
$$

It should be realized that the mean Rydberg population is enhanced by the intensity of the quantum fluctuation $\langle \delta \hat{\alpha}^\dagger \delta \hat{\alpha} \rangle$ induced by the Rydberg-Rydberg interaction. Moreover, the Mandel Q parameter is additionally affected by the quantum fluctuation $\langle \delta \hat{\alpha}^2 \rangle$ around $\langle b \rangle$. The cooperation of the quantum fluctuations $\langle \delta \hat{\alpha}^2 \rangle$ and $\langle \delta \hat{\alpha}^\dagger \delta \hat{\alpha} \rangle$ finally determines the statistical

dynamics of the Rydberg excitation, in relation to the super- (sub-)Poissonian counting statistics. On the other hand, the Hurwitz criterion for stability is given by $\Lambda > 0$. While Λ approaches zero, the quantum fluctuations diverge, and the linearization fails.

APPENDIX C: THE EXACT SOLUTION OF THE FOKKER-PLANCK EQUATION

Consider the Fokker-Planck equation (in the quantum noise limit, excluding the thermal noise, i.e., $n_{\mathrm{th}} = 0$)

$$
\dot{P}(\alpha, \beta, t) = \left[\partial_u \mathbf{A}_u(\alpha, \beta) + \tfrac{1}{2} \partial_u \partial_v \mathbf{D}_{uv}(\alpha, \beta) \right] P(\alpha, \beta, t)
$$

$$
= \partial_u \left\{ \tfrac{1}{2} \mathbf{D}_{uv} [(\mathbf{D}_{vu})^{-1} (2\mathbf{A}_u + \partial_v \mathbf{D}_{uv}) P + \partial_v P] \right\} \tag{C1}
$$

where $u, v = \alpha, \beta$ and the diffusion array is

$$
\mathbf{D}(\alpha, \beta) = \begin{bmatrix} -i\chi\alpha^2 & 0 \\ 0 & i\chi\beta^2 \end{bmatrix}, \tag{C2}
$$

$$
\mathbf{A}(\alpha, \beta) = \begin{bmatrix} i(\Gamma\alpha + \chi\alpha^2\beta + \lambda) \\ -i(\Gamma^*\beta + \chi\beta^2\alpha + \lambda) \end{bmatrix}. \tag{C3}
$$

A steady-state exact solution for the Fokker-Planck equation exists only when the conditional equations $\partial_u V_v = \partial_v V_u$ are fulfilled [56], where the potential function is given by $V_\varrho = (\mathbf{D}_{\varrho u})^{-1} (2\mathbf{A}_u + \partial_\sigma \mathbf{D}_{u\sigma})$, $\varrho = 1, 2$, that is,

$$
\begin{bmatrix} V_1 \\ V_2 \end{bmatrix} = -\frac{2}{\chi} \begin{bmatrix} (\Gamma - \chi)/\alpha + \chi\beta + \lambda/\alpha^2 \\ (\Gamma^* - \chi)/\beta + \chi\alpha + \lambda/\beta^2 \end{bmatrix}. \tag{C4}
$$

It is straightforward to verify that $\partial_\beta V_1 = \partial_\alpha V_2 = -2$ here. Thus, in the stationary limit $\dot{P}(\alpha, \beta, t = \infty) = 0$, we have

$$
\left[\partial_u \mathbf{A}_u(\alpha, \beta) + \tfrac{1}{2} \partial_u \partial_v \mathbf{D}_{uv}(\alpha, \beta) \right] P(\alpha, \beta, t) = 0 \tag{C5}
$$

or

$$
\partial_u \{ \mathbf{D}_{uv} [(\mathbf{D}_{vu})^{-1} (2\mathbf{A}_u + \partial_v \mathbf{D}_{uv}) P + \partial_v P] \} = 0. \tag{C6}
$$

The exact solution for the Fokker-Planck equation is therefore given by

$$
P_{ss}(\alpha, \beta) = \exp \left[-\int^{(\mathbb{C}_\alpha, \mathbb{C}_\beta)_\varrho} \mathbf{V}_\varrho(\alpha, \beta) d(\alpha, \beta)_\varrho \right]
$$

$$
= \exp \left\{ \frac{2}{\chi} \int^{\mathbb{C}_\alpha} [(\Gamma - \chi)/\alpha + \chi\beta + \lambda/\alpha^2] d\alpha \right.
$$

$$
\left. + \frac{2}{\chi} \int^{\mathbb{C}_\beta} [(\Gamma^* - \chi)/\beta + \chi\alpha + \lambda/\beta^2] d\beta \right\}
$$

$$
= \exp \left\{ \frac{2}{\chi} [(\Gamma - \chi) \ln \alpha - \lambda/\alpha] + \frac{2}{\chi} [(\Gamma^* - \chi) \ln \beta \right.
$$

$$
\left. - \lambda/\beta] + 2 \int^{(\mathbb{C}_\alpha, \mathbb{C}_\beta)} (\alpha d\beta + \beta d\alpha) \right\}
$$

$$
= \alpha^{c-2} \beta^{d-2} \exp[-z(1/\alpha + 1/\beta) + 2\alpha\beta], \tag{C7}
$$

where $z = 2\lambda/\chi$ and $c = 2\Gamma/\chi$ ($d = c^*$) are dimensionless quantities. Note that no Glauber-Sudarshan $P(\alpha, \alpha^*)$ function exists in the steady state with $\beta = \alpha^*$ due to the diverging
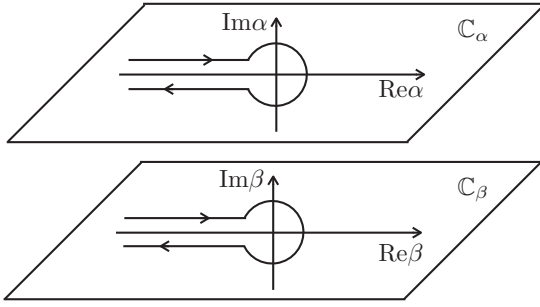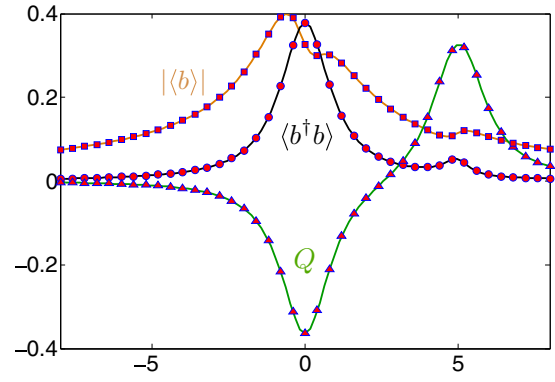
FIG. 6. The Hankel path of integration.

FIG. 7. Comparison of the numerical steady-state solution of $|\langle b \rangle|$, $\langle b^\dagger b \rangle$, and Q under the original master equation for the bosonization model (solid lines) with the analytical results (16)–(18) (symbols) in the main text. All parameters are the same as in Fig. 2(b).

exponential factor $\exp(2\alpha\alpha^*)$, except as a generalized form $P(\alpha,\beta)$.

The generalized $P(\alpha,\beta)$ function has to satisfy the normalization condition, which implies

$$
\begin{aligned}
I &= \int^{(\mathbb{C}_\alpha, \mathbb{C}_\beta)} P_{ss}(\alpha,\beta)\,d\alpha\,d\beta \\
&= \int^{(\mathbb{C}_\alpha, \mathbb{C}_\beta)} d\alpha\,d\beta\,\alpha^{c-2}\beta^{d-2}e^{-z(1/\alpha+1/\beta)+2\alpha\beta} \\
&= \int^{(\mathbb{C}_\alpha, \mathbb{C}_\beta)} d(\alpha^{-1})\,d(\beta^{-1}) \sum_{n=0}^{\infty} \frac{2^n}{n!}\alpha^{c+n}\beta^{d+n}e^{-z(1/\alpha+1/\beta)} \\
&= \int^{(\mathbb{C}_\alpha, \mathbb{C}_\beta)} d\alpha_1\,d\beta_1 \sum_{n=0}^{\infty} \frac{2^n}{n!}\alpha_1^{-(c+n)}\beta_1^{-(d+n)}e^{-z(\alpha_1+\beta_1)},
\end{aligned}
$$

(C8)

with $\alpha_1 = \alpha^{-1}$ and $\beta_1 = \beta^{-1}$. On the other hand, the Γ-function identity can be defined by using the Hankel path of integration $\mathcal{O}$ (see Fig. 6),

$$
\begin{aligned}
\frac{1}{\Gamma(c+n)} &= \frac{1}{2\pi i} \int_{\mathcal{O}} (\sigma z)^{-(c+n)} e^{\sigma z}\,d(\sigma z) \\
&= \frac{z^{1-(c+n)}}{2\pi i} \int_{\mathcal{O}} \sigma^{-(c+n)} e^{\sigma z}\,d\sigma,
\end{aligned}
$$

(C9)

with which we obtain

$$
\begin{aligned}
I &= \int^{(\mathbb{C}_\alpha, \mathbb{C}_\beta)} d\alpha_1\,d\beta_1 \sum_{n=0}^{\infty} \frac{2^n}{n!}\alpha_1^{-(c+n)}\beta_1^{-(d+n)}e^{-z(\alpha_1+\beta_1)} \\
&= \sum_{n=0}^{\infty} \frac{2^n}{n!}\left[\int_{\mathcal{O}} d\alpha_1 \alpha_1^{-(c+n)}e^{-z\alpha_1} \int_{\mathcal{O}} d\beta_1 \beta_1^{-(d+n)}e^{-z\beta_1}\right] \\
&= (-4\pi^2) \sum_{n=0}^{\infty} \frac{2^n}{n!}\frac{z^{c+d+2(n-1)}}{\Gamma(c+n)\Gamma(d+n)} \\
&= \frac{(-4\pi^2)z^{c+d-2}}{\Gamma(c)\Gamma(d)} {}_0F_2(c,d,2z^2),
\end{aligned}
$$

(C10)

where ${}_0F_2(c,d,z)$ is the generalized hypergeometric function defined as

$$
{}_0F_2(c,d,z) = \sum_{n=0}^{\infty} \frac{z^n}{n!}\frac{\Gamma(c)\Gamma(d)}{\Gamma(c+n)\Gamma(d+n)}.
$$

(C11)

The normalized ith-order correlation function $G^{(i,j)}$ corresponding to the normally ordered averages $\langle b^{\dagger i} b^j \rangle$ can be

calculated by the generalized P representation:

$$
\begin{aligned}
G^{(i,j)} &= \frac{\int d\sigma(\alpha,\beta)P(\alpha,\beta)\beta^m\alpha^n}{\int d\sigma(\alpha,\beta)P(\alpha,\beta)} \\
&= \frac{\frac{(-4\pi^2)z^{c+d-2+i+j}}{\Gamma(c+j)\Gamma(d+i)} {}_0F_2(c+j,d+i,2z^2)}{\frac{(-4\pi^2)z^{c+d-2}}{\Gamma(c)\Gamma(d)} {}_0F_2(c,d,2z^2)}.
\end{aligned}
$$

(C12)

With Euler's functional equation $\Gamma(z)/\Gamma(z+n+1) = 1/z(z+1)\cdots(z+n)$, we finally have

$$
G^{(i,j)} = z^{i+j} \frac{\Gamma(c)\Gamma(d) {}_0F_2(c+j,d+i,2z^2)}{\Gamma(c+j)\Gamma(d+i) {}_0F_2(c,d,2z^2)}
$$

(C13)

and therefore the quantum-mechanical steady-state solution of $\langle b \rangle$, $\langle b^\dagger b \rangle$, and $Q = \frac{\langle b^\dagger b^\dagger b b \rangle}{\langle b^\dagger b \rangle} - \langle b^\dagger b \rangle$. We have verified these analytical results by comparisons with the numerically obtained steady-state solution of the original master equation $\dot{\rho} = -i[H_b,\rho] + \frac{\gamma}{2}(2b\rho b^\dagger - \rho b^\dagger b - b^\dagger b \rho)$. As shown in Fig. 7, we find excellent agreement between the two different methods.

APPENDIX D: THE NONCLASSICAL NATURE OF THE QUANTUM-MECHANICAL STEADY STATES

The nonclassical nature of the quantum-mechanical steady states for the excitation processes with resonant driving and laser detuning $\Delta = \chi/2$ manifests itself in the Wigner function with a negative value, as shown in Fig. 8.
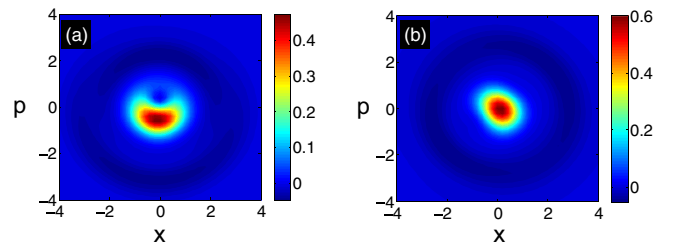

FIG. 8. Wigner function $W(x,p)$ of the quantum-mechanical steady-state solution with (a) $\Delta = 0$ and (b) $\Delta = \chi/2$.

[1] M. Saffman, T. G. Walker, and K. Mølmer, Rev. Mod. Phys. **82**, 2313 (2010).

[2] D. E. Chang, V. Vuletić, and M. D. Lukin, Nat. Photonics **8**, 685 (2014).

[3] J. D. Pritchard, D. Maxwell, A. Gauguet, K. J. Weatherill, M. P. A. Jones, and C. S. Adams, Phys. Rev. Lett. **105**, 193603 (2010).

[4] S. Sevinçli, N. Henkel, C. Ates, and T. Pohl, Phys. Rev. Lett. **107**, 153001 (2011).

[5] D. Petrosyan, J. Otterbach, and M. Fleischhauer, Phys. Rev. Lett. **107**, 213601 (2011).

[6] T. Peyronel, O. Firstenberg, Q.-Y. Liang, S. Hofferberth, A. V. Gorshkov, T. Pohl, M. D. Lukin, and V. Vuletić, Nature (London) **488**, 57 (2012).

[7] V. Parigi, E. Bimbard, J. Stanojevic, A. J. Hilliard, F. Nogrette, R. Tualle-Brouri, A. Ourjoumtsev, and P. Grangier, Phys. Rev. Lett. **109**, 233602 (2012).

[8] D. Yan, Y.-M. Liu, Q.-Q. Bao, C.-B. Fu, and J.-H. Wu, Phys. Rev. A **86**, 023828 (2012).

[9] A. V. Gorshkov, R. Nath, and T. Pohl, Phys. Rev. Lett. **110**, 153601 (2013).

[10] D. Maxwell, D. J. Szwer, D. Paredes-Barato, H. Busche, J. D. Pritchard, A. Gauguet, K. J. Weatherill, M. P. A. Jones, and C. S. Adams, Phys. Rev. Lett. **110**, 103001 (2013).

[11] B. He, A. V. Sharypov, J. Sheng, C. Simon, and M. Xiao, Phys. Rev. Lett. **112**, 133606 (2014).

[12] W. Li, D. Viscor, S. Hofferberth, and I. Lesanovsky, Phys. Rev. Lett. **112**, 243601 (2014).

[13] M. F. Maghrebi, M. J. Gullans, P. Bienias, S. Choi, I. Martin, O. Firstenberg, M. D. Lukin, H. P. Büchler, and A. V. Gorshkov, Phys. Rev. Lett. **115**, 123601 (2015).

[14] H. Weimer, R. Löw, T. Pfau, and H. P. Büchler, Phys. Rev. Lett. **101**, 250601 (2008).

[15] H. Weimer and H. P. Büchler, Phys. Rev. Lett. **105**, 230403 (2010).

[16] T. E. Lee, H. Häffner, and M. C. Cross, Phys. Rev. A **84**, 031402 (2011).

[17] J. Qian, G. Dong, L. Zhou, and W. Zhang, Phys. Rev. A **85**, 065401 (2012).

[18] I. Lesanovsky and J. P. Garrahan, Phys. Rev. Lett. **111**, 215305 (2013).

[19] M. Marcuzzi, E. Levi, S. Diehl, J. P. Garrahan, and I. Lesanovsky, Phys. Rev. Lett. **113**, 210401 (2014).

[20] M. Hoening, W. Abdussalam, M. Fleischhauer, and T. Pohl, Phys. Rev. A **90**, 021603 (2014).

[21] A. W. Glaetzle, R. Nath, B. Zhao, G. Pupillo, and P. Zoller, Phys. Rev. A **86**, 043403 (2012).

[22] M. Höning, D. Muth, D. Petrosyan, and M. Fleischhauer, Phys. Rev. A **87**, 023401 (2013).

[23] B. Vermersch, M. Punk, A. W. Glaetzle, C. Gross, and P. Zoller, New J. Phys. **17**, 013008 (2015).

[24] C. Ates, T. Pohl, T. Pattard, and J. M. Rost, Phys. Rev. Lett. **98**, 023002 (2007).

[25] C. Ates, T. Pohl, T. Pattard, and J. M. Rost, Phys. Rev. A **76**, 013413 (2007).

[26] M. Mayle, W. Zeller, N. Tezak, and P. Schmelcher, Phys. Rev. A **84**, 010701 (2011).

[27] C. Ates and I. Lesanovsky, Phys. Rev. A **86**, 013408 (2012).

[28] D. Petrosyan, M. Höning, and M. Fleischhauer, Phys. Rev. A **87**, 053414 (2013).

[29] M. Gärttner, K. P. Heeg, T. Gasenzer, and J. Evers, Phys. Rev. A **88**, 043410 (2013).

[30] S. Bettelli, D. Maxwell, T. Fernholz, C. S. Adams, I. Lesanovsky, and C. Ates, Phys. Rev. A **88**, 043436 (2013).

[31] J. Sanders, M. Jonckheere, and S. Kokkelmans, Phys. Rev. Lett. **115**, 043002 (2015).

[32] C. Ates, B. Olmos, J. P. Garrahan, and I. Lesanovsky, Phys. Rev. A **85**, 043620 (2012).

[33] T. E. Lee and M. C. Cross, Phys. Rev. A **85**, 063822 (2012).

[34] T. E. Lee, H. Häffner, and M. C. Cross, Phys. Rev. Lett. **108**, 023602 (2012).

[35] A. Hu, T. E. Lee, and C. W. Clark, Phys. Rev. A **88**, 053627 (2013).

[36] D. W. Schönleber, M. Gärttner, and J. Evers, Phys. Rev. A **89**, 033421 (2014).

[37] M. Gärttner, S. Whitlock, D. W. Schönleber, and J. Evers, Phys. Rev. Lett. **113**, 233002 (2014).

[38] B. Olmos, D. Yu, and I. Lesanovsky, Phys. Rev. A **89**, 023616 (2014).

[39] H. Weimer, Phys. Rev. A **91**, 063401 (2015).

[40] H. Schempp, G. Günter, S. Wüster, M. Weidemüller, and S. Whitlock, Phys. Rev. Lett. **115**, 093002 (2015).

[41] M. Viteau, P. Huillery, M. G. Bason, N. Malossi, D. Ciampini, O. Morsch, E. Arimondo, D. Comparat, and P. Pillet, Phys. Rev. Lett. **109**, 053002 (2012).

[42] C. S. Hofmann, G. Günter, H. Schempp, M. Robert-de-Saint-Vincent, M. Gärttner, J. Evers, S. Whitlock, and M. Weidemüller, Phys. Rev. Lett. **110**, 203601 (2013).

[43] C. Carr, R. Ritter, C. G. Wade, C. S. Adams, and K. J. Weatherill, Phys. Rev. Lett. **111**, 113901 (2013).

[44] H. Schempp, G. Günter, M. Robert-de Saint-Vincent, C. S. Hofmann, D. Breyel, A. Komnik, D. W. Schönleber, M. Gärttner, J. Evers, S. Whitlock *et al.*, Phys. Rev. Lett. **112**, 013002 (2014).

[45] A. Urvoy, F. Ripka, I. Lesanovsky, D. Booth, J. P. Shaffer, T. Pfau, and R. Löw, Phys. Rev. Lett. **114**, 203002 (2015).

[46] N. Malossi, M. M. Valado, S. Scotto, P. Huillery, P. Pillet, D. Ciampini, E. Arimondo, and O. Morsch, Phys. Rev. Lett. **113**, 023006 (2014).

[47] M. M. Valado, C. Simonelli, M. D. Hoogerland, I. Lesanovsky, J. P. Garrahan, E. Arimondo, D. Ciampini, and O. Morsch, Phys. Rev. A **93**, 040701(R) (2016).

[48] G. Günter, M. Robert-de-Saint-Vincent, H. Schempp, C. S. Hofmann, S. Whitlock, and M. Weidemüller, Phys. Rev. Lett. **108**, 013002 (2012).

[49] A. Schwarzkopf, R. E. Sapiro, and G. Raithel, Phys. Rev. Lett. **107**, 103001 (2011).

[50] P. D. Drummond and D. F. Walls, J. Phys. A **13**, 725 (1980).

[51] H. Labuhn, D. Barredo, S. Ravets, S. de Léséleuc, T. Macrì, T. Lahaye, and A. Browaeys, Nature (London) **534**, 667 (2016).

[52] J. W. Britton, B. C. Sawyer, A. C. Keith, C. C. J. Wang, J. K. Freericks, H. Uys, M. J. Biercuk, and J. J. Bollinger, Nature (London) **484**, 489 (2012).

[53] C. P. Sun, Y. Li, and X. F. Liu, Phys. Rev. Lett. **91**, 147903 (2003).

[54] K. Hammerer, A. S. Sørensen, and E. S. Polzik, Rev. Mod. Phys. **82**, 1041 (2010).

[55] S. Wüster, J. Stanojevic, C. Ates, T. Pohl, P. Deuar, J. F. Corney, and J. M. Rost, Phys. Rev. A **81**, 023406 (2010).

[56] H. Haken, Rev. Mod. Phys. **47**, 67 (1975).